



HAL
open science

Epsilon near-zero all-optical terahertz modulator

E. Alvear-Cabezón, T. Taliercio, S. Blin, R. Smaali, F. Gonzalez-Posada, A. Baranov, R. Teissier, E. Centeno

► **To cite this version:**

E. Alvear-Cabezón, T. Taliercio, S. Blin, R. Smaali, F. Gonzalez-Posada, et al.. Epsilon near-zero all-optical terahertz modulator. *Applied Physics Letters*, 2020, 117 (11), pp.111101. 10.1063/5.0012206 . hal-03009384

HAL Id: hal-03009384

<https://hal.science/hal-03009384>

Submitted on 11 Nov 2021

HAL is a multi-disciplinary open access archive for the deposit and dissemination of scientific research documents, whether they are published or not. The documents may come from teaching and research institutions in France or abroad, or from public or private research centers.

L'archive ouverte pluridisciplinaire **HAL**, est destinée au dépôt et à la diffusion de documents scientifiques de niveau recherche, publiés ou non, émanant des établissements d'enseignement et de recherche français ou étrangers, des laboratoires publics ou privés.

Epsilon near-zero all-optical terahertz modulator

Cite as: Appl. Phys. Lett. **117**, 111101 (2020); <https://doi.org/10.1063/5.0012206>

Submitted: 30 April 2020 . Accepted: 03 September 2020 . Published Online: 14 September 2020

E. Alvear-Cabezón , T. Taliercio , S. Blin , R. Smaali, F. Gonzalez-Posada , A. Baranov, R. Teissier, and E. Centeno 



View Online



Export Citation



CrossMark

HIDEN
ANALYTICAL

Instruments for Advanced Science

Contact Hiden Analytical for further details:

W www.HidenAnalytical.com

E info@hiden.co.uk

CLICK TO VIEW our product catalogue



Gas Analysis

- dynamic measurement of reaction gas streams
- catalysis and thermal analysis
- molecular beam studies
- dissolved species probes
- fermentation, environmental and ecological studies



Surface Science

- UHV TPD
- SIMS
- end point detection in ion beam etch
- elemental imaging - surface mapping



Plasma Diagnostics

- plasma source characterization
- etch and deposition process reaction kinetic studies
- analysis of neutral and radical species



Vacuum Analysis

- partial pressure measurement and control of process gases
- reactive sputter process control
- vacuum diagnostics
- vacuum coating process monitoring



Epsilon near-zero all-optical terahertz modulator

Cite as: Appl. Phys. Lett. **117**, 111101 (2020); doi: [10.1063/5.0012206](https://doi.org/10.1063/5.0012206)

Submitted: 30 April 2020 · Accepted: 3 September 2020 ·

Published Online: 14 September 2020



View Online



Export Citation



CrossMark

E. Alvear-Cabezón,^{1,2,a)}  T. Taliercio,²  S. Blin,²  R. Smaali,¹ F. Gonzalez-Posada,²  A. Baranov,² R. Teissier,² and E. Centeno^{1,a)} 

AFFILIATIONS

¹Université Clermont Auvergne, CNRS, SIGMA Clermont, Institut Pascal, F-63000 Clermont-Ferrand, France

²IES, Univ Montpellier, UMR CNRS 5214, Montpellier, France

^{a)}Authors to whom correspondence should be addressed: eduardo.alvear10@gmail.com and emmanuel.centeno@uca.fr

ABSTRACT

We propose an efficient optically actuated THz modulator based on an ultrathin epsilon-near-zero (ENZ) slab photogenerated in an InAs semiconductor. We experimentally demonstrate a modulation depth of 90% at 1 THz obtained with a continuous laser at irradiation lower than 10 W cm^{-2} . Beyond the strong attenuation of the THz transmission provided by the ENZ absorption effect, we also report a broadband modulation of the THz waves from 1 to 10 THz. In addition, our experimental results show that the cut-off frequency of 3 dB attains 2 MHz in the dynamic modulation regime.

Published under license by AIP Publishing. <https://doi.org/10.1063/5.0012206>

The development of the technology based on terahertz (THz) electromagnetic radiation is crucial for many application domains such as security, medicine, and wireless communication.^{1–6} The demand for versatile THz components operating in the THz gap (0.1–10 THz) is high. Artificial structures such as metasurfaces have been recently investigated to dynamically control THz waves.^{7–9} Thermal, mechanical, electrical, and optical actuations have been explored to reach an efficient and high speed modulation of THz signals. Comparison between these approaches can be found in several reviews, see, for example, Table I of Refs. 10 and 11. Among those approaches, all-optical devices have attracted great interest since they provide a high modulation depth. Photocarriers are generated within a semiconductor, such as silicon, GaAs, and Ge, when it is illuminated by a pump beam. This excess of carriers modifies the mobility and/or the conductivity of the material, which is probed by the THz signal. To improve the modulation depth and lower the pump power, 2D materials such as graphene have been deposited on such semiconductors.¹² In that case, a modulation depth up to 94% has been reached but for a low modulation speed of 200 kHz and in a broadband range lower than 1 THz.¹³ Comparison of these optically actuated THz modulators is reviewed in Refs. 11 and 14. Usually, the resonant behavior of metasurfaces limits the modulation of the THz signal over a wide broadband of frequency. Photo-generated metasurfaces have been developed to overcome this limitation. In that case, a pump laser induces a local refractive index modification into a semiconductor layer, leading to optically printed metasurfaces.^{15–21} The design is scaled according to the targeted THz frequency, which provides an optimal

modulation. The main issue that prevents the implementation of all-optical THz modulators in the application domain concerns the high pump power required to modulate efficiently the THz signal. However, recent theoretical results suggest that Indium Arsenide (InAs) is a promising semiconductor to realize high THz modulation using a low pump power in the continuous-wave (CW) regime.^{22,23} Recent studies demonstrate that perfect absorption also occurs within a slab when the real part of the permittivity approaches zero. It has been demonstrated that epsilon-near zero (ENZ) modes efficiently absorb the incoming radiation in an ultrathin slab, presenting very small optical losses.^{24–27} An additional coupling device is needed to excite such ENZ guided modes by using resonators or a prism in the Kretschmann–Raether configuration.^{28–30} Moreover, several works have demonstrated that the ENZ frequency can be dynamically varied with transparent conductive oxides (for example, indium tin oxide, ITO) or with doped semiconductors.^{28–30} In that case, an applied voltage modifies the electronic density, which, in turn, shifts the ENZ frequency. The maximum frequency shift of the absorption peak experimentally observed attains 20% for a modulation depth of about 20% and a 125 kHz modulation rate.²⁹ No matter how these approaches are implemented, the modulation of the THz signal depends on the strength of the coupling between the THz waves and the active material. This condition is usually reached by properly designing the metasurface (such as the size and the shape of the resonators).^{31,32} Finally, efficient THz modulators are generally complex systems, not always CMOS compatible and operates in a narrow frequency range and sometime at very low temperature. In this work, we

propose a very simple all-optical THz modulator based on an InAs slab. We demonstrate a modulation depth up to 90% at 1 THz for a low pump irradiance of 8.1 W cm^{-2} in the continuous-wave regime. The optically induced modification of the refractive index produces a broadband modulation of the THz transmission from 1 THz to 10 THz. In addition, a modulation speed up to 2 MHz is experimentally demonstrated in the pulse regime. The InAs semiconductor is an attractive material, compatible with the CMOS technology and operating at room temperature.³³ In addition, the modulator is very compact since the thickness of the InAs slab is about $\lambda/50$. This efficient absorption within an ultrathin slab is explained by the photogeneration of an ENZ material.

The sample used in this work is a free-standing InAs slab of $6 \mu\text{m}$ thickness. Its preparation needs the following steps: a $15 \mu\text{m}$ thick layer of an undoped InAs and a thin layer of 300 nm of AlAsSb (etch-stop) are deposited by solid-source molecular beam epitaxy on a doped InAs substrate. After a partial polishing of the InAs substrate, the undoped InAs layer is stuck using an epoxy adhesive (ECCOBOND 144A) to a sample holder of copper covered by a thin gold layer. Then, the rest of the InAs substrate is chemically etched by a solution of citric acid diluted in hydrogen peroxide [$\text{C}_6\text{H}_8\text{O}_7 : \text{H}_2\text{O}_2$ (2:1)]. The etching process stops on the AlAsSb layer thanks to the selective etching between AlAsSb and InAs.³⁴ Finally, the AlAsSb layer is removed with a HF buffer and the InAs slab is progressively thinned by using a solution of phosphoric acid diluted in hydrogen peroxide and water [$\text{H}_3\text{PO}_4 : \text{H}_2\text{O}_2 : \text{H}_2\text{O}$ (2:1:1)] up to $6 \mu\text{m}$. The InAs slab covers a 2 mm hole of the sample holder. The slab thickness is controlled by transmission experiments from 1 to 10 THz (Fig. 1) using a Bruker Vertex 70 Fourier transform infrared (FTIR) spectrometer equipped with a water-cooled far-infrared light-source, a Si-beam splitter, and a cooled Si bolometer. The FTIR experiments are done under N_2 flux. All the spectra are numerically smoothed to remove absorption lines from residual gases other than N_2 in the FTIR spectrometer. We used an 808 nm laser with a collimated beam, with a diameter larger than the hole of the sample holder and a tunable irradiance to photogenerate free carriers in the InAs slab. The transmission spectrum with null irradiance in Fig. 1 shows interference fringes allowing us to adjust our model using only the thickness as a

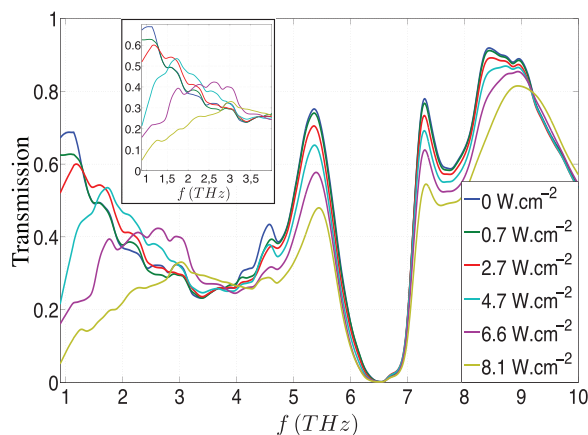


FIG. 1. Experimental transmission spectra for various pump irradiance values $\Phi_0 : \{0, 0.7, 2.7, 4.7, 6.6, 8.1\} \text{ W cm}^{-2}$. The inset represents a zoom of the spectra.

parameter. Without the laser pump, the transmission peaks originating from Fabry-Pérot (FP) resonances arise around 1, 5.5, 7.25, and 8.3 THz. The THz wave is reflected in the *Reststrahlen* phonon band in the range of 6–7 THz. Several modifications appear in the transmission spectrum as the laser pump irradiance denoted as Φ_0 increases from 0 to 8.1 W cm^{-2} . In the range of 1–4 THz, we observe a shift and a broadening of the main transmission peak. Besides, the transmission is substantially modulated (up to 30%) at the FP resonances (5.5, 7.25, and 8.3 THz) since the dielectric function is significantly modified.

The optical modulation of the THz signal for a very low pump irradiance is clearly demonstrated by representing the relative transmission modulation defined as $(T_{\text{off}} - T_{\text{on}})/T_{\text{off}}$ where T_{off} and T_{on} are the transmission spectra when the pump is turned off ($\Phi_0 = 0$) and on, respectively (Fig. 2). The maximal modulation depth attains 90% at 1 THz for $\Phi_0 = 8.1 \text{ W cm}^{-2}$. This very low pump irradiance produces a drastic change for the THz transmission that decreases from 69% to 7%. This high modulation occurs for a wavelength fifty times larger than the InAs layer thickness. The modulation attains 42%, 32%, and 27% at the respective FP resonances 5.5, 7.25, and 8.3 THz. The modulation is not considered in the *Reststrahlen* phonon band since the transmission is close to zero in this range independently of the pump power.

To understand these results, the permittivity of the InAs slab is modeled by combining a Lorentz model for the phonon resonances and a Drude model for the free-carrier effect,

$$\epsilon_m = \epsilon_\infty \left(1 - \frac{\omega_p(n)^2}{\omega(\omega + i\gamma)} + \frac{\omega_{LO}^2 - \omega_{TO}^2}{\omega_{TO}^2 - \omega^2 - i\omega\Gamma} \right), \quad (1)$$

where $\epsilon_\infty = 12.32$, $\omega_{LO} = 45 \times 10^{12} \text{ rad s}^{-1}$, $\omega_{TO} = 40 \times 10^{12} \text{ rad s}^{-1}$, $\Gamma = 0.56 \times 10^{12} \text{ rad s}^{-1}$. The angular plasma frequency $\omega_p(n)$ for the Drude model is a function of the carrier density n ,

$$\omega_p(n) = \sqrt{ne^2 / (m_{\text{eff}}\epsilon_0\epsilon_\infty)}. \quad (2)$$

The damping coefficient is $\gamma = e/(\mu m_{\text{eff}})$, where $m_{\text{eff}} = 0.024m_e$ is the electron's effective mass (with m_e being the electron mass) and $\mu = 24\,000 \text{ cm}^2 \text{ V}^{-1} \text{ s}^{-1}$ the electronic mobility.

The laser pump photogenerates electron-hole pairs that diffuse together within the InAs slab. This carrier density n obeys to an

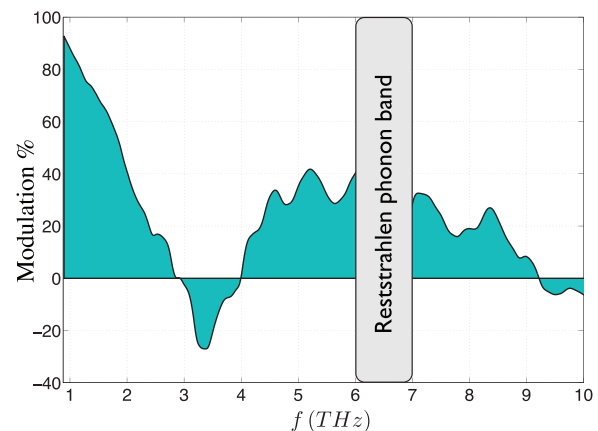


FIG. 2. Relative transmission modulation of an undoped $6 \mu\text{m}$ thick InAs slab irradiated with a pump irradiance of 8.1 W cm^{-2} at room temperature.

ambipolar transport equation that is solved following the calculations presented in Ref. 22. We consider an intrinsic doping $n_0 = 2 \times 10^{15} \text{ cm}^{-3}$.

With this model, the permittivity derived from Eq. (1) is calculated when the pump switches from off to on (Fig. 3). Without the optical pumping, the real part of the permittivity vanishes for two ENZ frequencies: around the plasma frequency of $f_p = \omega_p/2\pi$ at 0.48 THz and at the longitudinal optical phonon frequency of $f_{LO} = 7.2$ THz. When the pump is turned on ($\Phi_0 = 8.1 \text{ W cm}^{-2}$), the plasma frequency shifts to $f_p = 1.75$ THz. According to Eq. (2), the increase in the photogenerated carrier density causes the increase in the plasma frequency. Beyond the control over the plasma frequency allowed by the optical pump, the permittivity is globally modified at higher frequencies. Indeed, the Drude term in Eq. (1) introduces changes in both the real and imaginary parts that affect the overall permittivity. These modifications are directly responsible for the modulation of the THz signal in the range of 2–10 THz. From this permittivity model, we are able to calculate the THz transmission as a function of the pump irradiance (Fig. 4). These calculations fairly reproduce the experimental data with, in particular, the shift of the first transmission peak from 1 THz to 2.5 THz. We calculate the THz absorption for varying pump irradiance to understand the evolution of the THz transmission (Fig. 5). In the range of 1–2 THz, both absorption and transmission (solid line) peaks follow the shift experienced by the ENZ frequency (dashed line). According to Eq. (2), the increase in the carrier density is responsible for the plasma frequency shift and consequently the shift of the ENZ frequency. The slab acts like a Fabry-Pérot cavity that supports resonances, which can be either symmetric or anti-symmetric with respect to the middle of the slab. When the wavelength is large compared to the slab thickness, the fundamental symmetric resonance is predominant. In this case, the amplitude of the reflected wave can be written as

$$R = A \frac{e^{2ik_0\bar{n}h} - r}{1 - re^{2ik_0\bar{n}h}}, \quad (3)$$

where A is the incident amplitude, $r = (1 - \bar{n})/(1 + \bar{n})$ and $t = 1 + r$ are the Fresnel coefficients, and $\bar{n} = n + i\kappa$ is the complex refractive

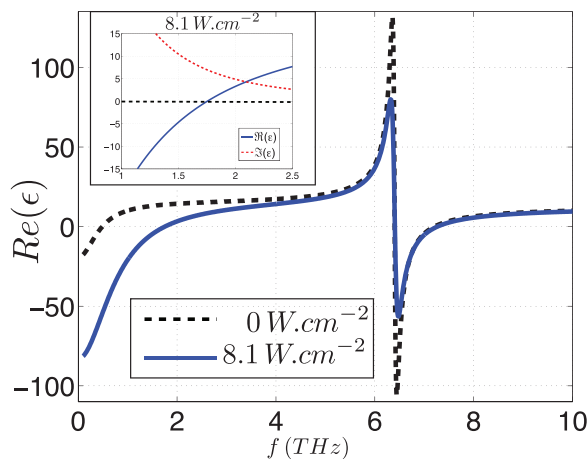


FIG. 3. Real part of the InAs permittivity for $\Phi_0 = 0 \text{ W cm}^{-2}$ (dashed curve) and $\Phi_0 = 8.1 \text{ W cm}^{-2}$ (solid curve). The inset shows the real and imaginary parts of the permittivity around the plasma frequency for $\Phi_0 = 8.1 \text{ W cm}^{-2}$.

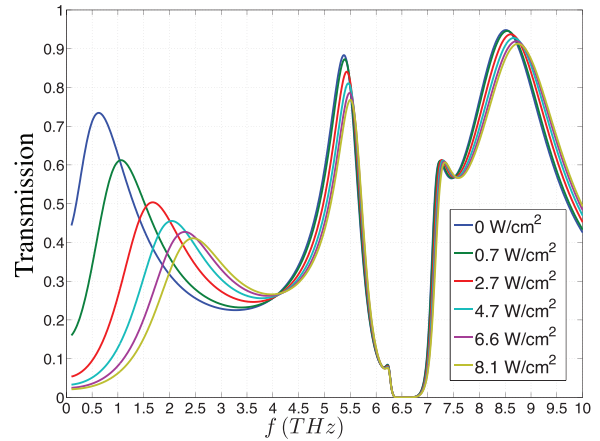


FIG. 4. Theoretical transmission spectra for increasing pump irradiance, $\Phi_0 : \{0, 0.7, 2.7, 4.7, 6.6, 8.1\} \text{ W cm}^{-2}$.

index of InAs. The absorption of the THz wave is maximal when the reflection is null, which leads to a reflection coefficient of zero. After some analytical derivations, the thickness of the slab that satisfies this criterion is

$$h = \frac{\lambda}{2\pi n} \arctan\left(\frac{2\kappa}{n^2 + \kappa^2 - 1}\right). \quad (4)$$

At the ENZ frequency, the refractive index and absorption coefficients are equal and only determined by the imaginary part of the permittivity, $n_0 = \kappa_0 = \sqrt{\Im(\epsilon_m)}/2$ (see the inset of Fig. 3). In our case, κ_0 is larger than one, which allows us to evaluate the optimal InAs thickness $h_0 \approx \lambda/(\pi\Im(\epsilon_m))$. From Eq. (1), we estimate that the optimal thickness is about 5 to 10 μm for a carrier density between 10^{15} cm^{-3} and 10^{16} cm^{-3} . The photogenerated ENZ material enhances the THz absorption around 1 THz within a $\lambda/50$ thick InAs slab. In agreement with the result of Fig. 5, the frequency shift of the THz transmission

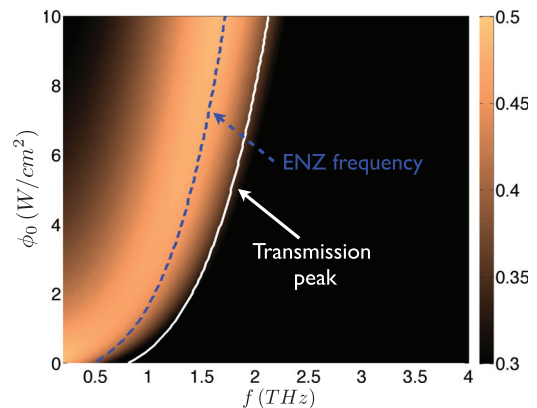


FIG. 5. Theoretical absorption as a function of the THz frequency and the irradiance. The dashed line represents the position of the plasma frequency, and the solid line corresponds to the transmission peak.

originates, hence, from this ENZ absorption mechanism that occurs close to the plasma frequency, which is optically tuned.

To evaluate the dynamic performances of the InAs slab for THz amplitude modulation, we used the experimental setup shown in Fig. 6 and described in the figure caption. The principle of the measurements consists of the observation of the transmitted THz spectrum through the InAs slab illuminated by a laser beam sinusoidally modulated at increasing frequencies f_m . The laser beam irradiance is modulated by an acousto-optic modulator that attains a maximal value of 2.5 W cm^{-2} . This optical excitation leads to a dynamic behavior of the permittivity that can be written as $\varepsilon(t) = \varepsilon + \Delta\varepsilon(f_m) \cos(2\pi f_m t)$. The amplitude of the perturbation $\Delta\varepsilon$ depends on the efficiency of the photogeneration process, which is limited by the recombination time τ_r . The transfer function of the photogenerated carrier density corresponds to a first-order low-pass filter $1/\sqrt{1 + (2\pi f_m \tau_r)^2}$. The oscillating behavior of the permittivity value leads to an amplitude modulation of the THz signal, and therefore, sidebands at $f_0 \pm f_m$ appear in the THz spectrum as shown in the inset of Fig. 7 for $f_m = 5 \text{ kHz}$ and for an incident THz

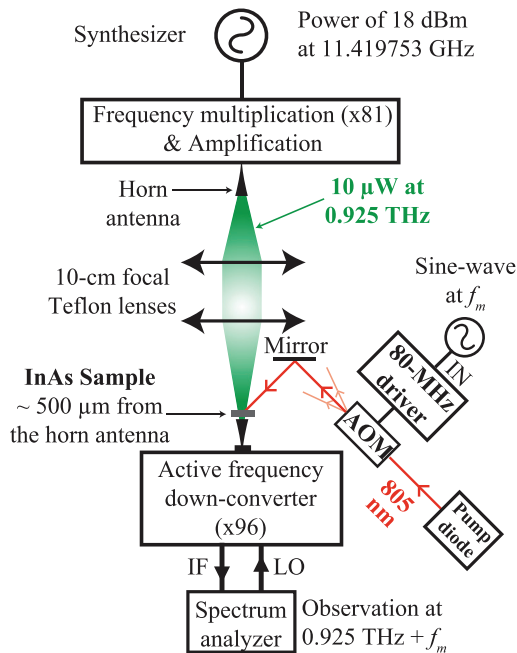


FIG. 6. Experimental setup implemented to study the dynamic THz transmission at 0.925 THz through a $6 \mu\text{m}$ -thick InAs slab photo-excited by a 808 nm laser pump. This 500 mW laser has an amplitude modulated by a 80 MHz acousto-optic modulator (AOM). The THz source consists of a frequency-multiplied chain (from VDI Inc.) driven by a synthesizer. The waveguide output permits the propagation of frequencies from 0.75 to 1.10 THz with an output power close to $10 \mu\text{W}$. A horn antenna is used at the waveguide output to reduce diffraction, and a couple of 10-cm-focal-length Teflon lenses is used to focus the THz signal into a THz heterodyne detector. This detector consists of an active frequency down-converter chain (from RPI Inc.) driven by the local oscillator of an electrical spectrum analyzer. Thanks to a multiplication factor of $96\times$, the local oscillator mixes with the incoming THz signal at the front-end Schottky diode of the down-converter chain, thus producing a low-intermediate frequency that is detected by the spectrum analyzer. The input THz power is collected with a horn antenna. The InAs slab is located as close as possible (about $500 \mu\text{m}$) in front of the receiver horn antenna.

signal of frequency $f_0 = 0.925 \text{ THz}$. Remark that high frequency modulation of the permittivity is responsible for non-reciprocal behavior of light in current photonic devices.^{35,36} The cut-off frequency is measured by monitoring the amplitude of the satellite THz signal at the frequency $f_0 + f_m$ as the modulation frequency of the pump f_m is increased (see the inset of Fig. 7). The accuracy of the spectrum measurement observed using a frequency-swept analyzer is strongly degraded by the frequency noise related to the extreme frequency multiplication factors that are involved at both the source ($\times 81$) and detection ($\times 96$) sides. Therefore, for each modulation frequency, we acquired 20 spectra centered at $f_0 + f_m$ with a span of 1 kHz and only retained the maximum amplitude in a post-processing analysis.

The transfer function of the InAs slab is extracted from these measurements, after being corrected by the AOM transfer function that was preliminarily measured (Fig. 7). According to the photogeneration dynamics, the THz response of the InAs film can be fitted (red curve) by a first-order low-pass filter whose experimental cut-off frequency is 2 MHz. We remark that the transfer function drops below the fit at high modulation frequencies (above few MHz) since the average pump irradiance reduces as the modulation frequency increases.

In conclusion, we have demonstrated that an ENZ absorption effect achieved in a sub-wavelength InAs slab leads to a high modulation of the THz signal. In the continuous regime, the modulation depth attains 90% at 1 THz. Beyond this resonant ENZ modulation, the THz signal is also modulated in a broadband of frequency from 2 to 10 THz at the Fabry-Pérot resonances. This THz modulator is optically actuated by a laser pump of irradiance lower than 10 W cm^{-2} and works at room temperature. In the dynamic regime, the optical actuation is demonstrated to be efficient until a frequency of 2 MHz. These theoretical and experimental results open up possibilities for a

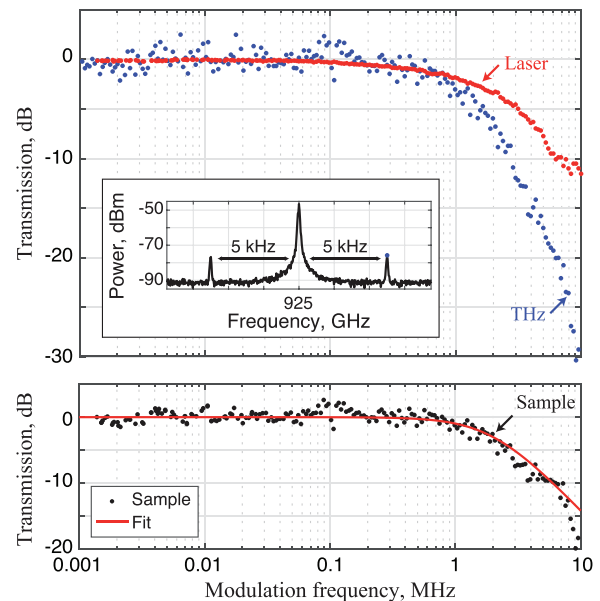


FIG. 7. The transfer function of the InAs slab: the dots correspond to the experimental data and the solid line to their fit with a first-order low pass filter. The inset of the figure shows the THz spectrum measured using a 10 Hz resolution bandwidth for a laser amplitude modulation frequency of $f_m = 5 \text{ kHz}$.

new concept of pure phase/amplitude THz spatial modulator for single-pixel THz imaging.

This work was partially funded by the French Investment for the Future program (EquipEx EXTRA, No. ANR 11-EQPX-0016). This work was funded by the French Labex IMOBS3.

DATA AVAILABILITY

The data that support the findings of this study are available from the corresponding author upon reasonable request.

REFERENCES

- ¹S. Dhillon, M. Vitiello, E. Linfield, A. Davies, M. C. Hoffmann, J. Booske, C. Paoloni, M. Gensch, P. Weightman, G. Williams *et al.*, “The 2017 terahertz science and technology roadmap,” *J. Phys. D: Appl. Phys.* **50**, 043001 (2017).
- ²Y.-S. Lee, *Principles of Terahertz Science and Technology* (Springer Science & Business Media, 2009), Vol. 170.
- ³J. F. Federici, B. Schulkin, F. Huang, D. Gary, R. Barat, F. Oliveira, and D. Zimdars, “Thz imaging and sensing for security applications—explosives, weapons and drugs,” *Semicond. Sci. Technol.* **20**, S266 (2005).
- ⁴M. Tonouchi, “Cutting-edge terahertz technology,” *Nat. Photonics* **1**, 97 (2007).
- ⁵K. Zaitsev, N. Chernomyrdin, K. Kudrin, I. Reshetov, and S. Yurchenko, “Terahertz spectroscopy of pigmentary skin nevi in vivo,” *Opt. Spectrosc.* **119**, 404–410 (2015).
- ⁶S. Koenig, D. Lopez-Diaz, J. Antes, F. Boes, R. Henneberger, A. Leuther, A. Tessmann, R. Schmogrow, D. Hillerkuss, R. Palmer *et al.*, “Wireless sub-THz communication system with high data rate,” *Nat. Photonics* **7**, 977–981 (2013).
- ⁷H.-T. Chen, A. J. Taylor, and N. Yu, “A review of metasurfaces: Physics and applications,” *Rep. Prog. Phys.* **79**, 076401 (2016).
- ⁸K. Fan and W. J. Padilla, “Dynamic electromagnetic metamaterials,” *Mater. Today* **18**, 39–50 (2015).
- ⁹H.-T. Chen, W. J. Padilla, J. M. Zide, A. C. Gossard, A. J. Taylor, and R. D. Averitt, “Active terahertz metamaterial devices,” *Nature* **444**, 597 (2006).
- ¹⁰L. Wang, Y. Zhang, X. Guo, T. Chen, H. Liang, X. Hao, X. Hou, W. Kou, Y. Zhao, T. Zhou *et al.*, “A review of thz modulators with dynamic tunable metasurfaces,” *Nanomaterials* **9**, 965 (2019).
- ¹¹R. Degl’Innocenti, S. J. Kindness, H. E. Beere, and D. A. Ritchie, “All-integrated terahertz modulators,” *Nanophotonics* **7**, 127–144 (2018).
- ¹²S. Yu, X. Wu, Y. Wang, X. Guo, and L. Tong, “2D materials for optical modulation: Challenges and opportunities,” *Adv. Mater.* **29**, 1606128 (2017).
- ¹³Q.-Y. Wen, W. Tian, Q. Mao, Z. Chen, W.-W. Liu, Q.-H. Yang, M. Sanderson, and H.-W. Zhang, “Graphene based all-optical spatial terahertz modulator,” *Sci. Rep.* **4**, 7409 (2015).
- ¹⁴Z. Ma, Z. Geng, Z. Fan, J. Liu, and H. Chen, “Modulators for terahertz communication: The current state of the art,” *Research* **2019**, 1.
- ¹⁵T. Okada and K. Tanaka, “Photo-designed terahertz devices,” *Sci. Rep.* **1**, 121 (2011).
- ¹⁶X. Wang, Z. Xie, W. Sun, S. Feng, Y. Cui, J. Ye, and Y. Zhang, “Focusing and imaging of a virtual all-optical tunable terahertz fresnel zone plate,” *Opt. Lett.* **38**, 4731–4734 (2013).
- ¹⁷G. Georgiou, H. Tyagi, P. Mulder, G. Bauhuis, J. Schermer, and J. G. Rivas, “Photo-generated THz antennas,” *Sci. Rep.* **4**, 3584 (2015).
- ¹⁸T. P. Steinbusch, H. K. Tyagi, M. C. Schaafsma, G. Georgiou, and J. G. Rivas, “Active terahertz beam steering by photo-generated graded index gratings in thin semiconductor films,” *Opt. Express* **22**, 26559–26571 (2014).
- ¹⁹G. Georgiou, C. Tserkezis, M. Schaafsma, J. Aizpurua, and J. G. Rivas, “Active loaded plasmonic antennas at terahertz frequencies: Optical control of their capacitive-inductive coupling,” *Phys. Rev. B* **91**, 125443 (2015).
- ²⁰Y. Yang, N. Kamaraju, S. Campione, S. Liu, J. L. Reno, M. B. Sinclair, R. P. Prasankumar, and I. Brener, “Transient gas plasmonic metasurfaces at terahertz frequencies,” *ACS Photonics* **4**, 15–21 (2017).
- ²¹C. Rizza, A. Ciattoni, L. Columbo, M. Brambilla, and F. Prati, “Terahertz optically tunable dielectric metamaterials without microfabrication,” *Opt. Lett.* **38**, 1307–1309 (2013).
- ²²E. Alvear-Cabezón, R. Smaali, E. Centeno, F. Gonzalez-Posada, and T. Taliercio, “Photogenerated metasurfaces at terahertz frequencies induced by a continuous-wave low pump,” *Phys. Rev. B* **98**, 035305 (2018).
- ²³H. R. Seren, J. Zhang, G. R. Keiser, S. J. Maddox, X. Zhao, K. Fan, S. R. Bank, X. Zhang, and R. D. Averitt, “Nonlinear terahertz devices utilizing semiconducting plasmonic metamaterials,” *Light: Sci. Appl.* **5**, e16078 (2016).
- ²⁴Y. Jin, S. Xiao, N. A. Mortensen, and S. He, “Arbitrarily thin metamaterial structure for perfect absorption and giant magnification,” *Opt. Express* **19**, 11114–11119 (2011).
- ²⁵S. Feng and K. Halterman, “Coherent perfect absorption in epsilon-near-zero metamaterials,” *Phys. Rev. B* **86**, 165103 (2012).
- ²⁶T. S. Luk, S. Campione, I. Kim, S. Feng, Y. C. Jun, S. Liu, J. B. Wright, I. Brener, P. B. Catrysse, S. Fan *et al.*, “Directional perfect absorption using deep subwavelength low-permittivity films,” *Phys. Rev. B* **90**, 085411 (2014).
- ²⁷S. Campione, I. Brener, and F. Marquier, “Theory of epsilon-near-zero modes in ultrathin films,” *Phys. Rev. B* **91**, 121408 (2015).
- ²⁸J. Park, J.-H. Kang, X. Liu, and M. L. Brongersma, “Electrically tunable epsilon-near-zero (ENZ) metafilm absorbers,” *Sci. Rep.* **5**, 15754 (2015).
- ²⁹A. Anopchenko, L. Tao, C. Arndt, and H. W. H. Lee, “Field-effect tunable and broadband epsilon-near-zero perfect absorbers with deep subwavelength thickness,” *ACS Photonics* **5**, 2631–2637 (2018).
- ³⁰Y. C. Jun, J. Reno, T. Ribaudou, E. Shaner, J.-J. Greffet, S. Vassant, F. Marquier, M. Sinclair, and I. Brener, “Epsilon-near-zero strong coupling in metamaterial-semiconductor hybrid structures,” *Nano Lett.* **13**, 5391–5396 (2013).
- ³¹S. Collin, “Nanostructure arrays in free-space: Optical properties and applications,” *Rep. Prog. Phys.* **77**, 126402 (2014).
- ³²R. Smaali, F. Omeis, A. Moreau, T. Taliercio, and E. Centeno, “A universal design to realize a tunable perfect absorber from infrared to microwaves,” *Sci. Rep.* **6**, 32589 (2016).
- ³³T. Taliercio and P. Biagioni, “Semiconductor infrared plasmonics,” *Nanophotonics* **8**, 949 (2019).
- ³⁴G. C. Desalvo, R. Kaspi, and C. A. Bozada, “Citric acid etching of GaAs_xSb_x, Al_{0.5}Ga_{0.5}Sb, and InAs for heterostructure device fabrication,” *J. Electrochem. Soc.* **141**, 3526 (1994).
- ³⁵D. L. Sounas and A. Alù, “Non-reciprocal photonics based on time modulation,” *Nat. Photonics* **11**, 774–783 (2017).
- ³⁶K. Fang, Z. Yu, and S. Fan, “Photonic aharonov-bohm effect based on dynamic modulation,” *Phys. Rev. Lett.* **108**, 153901 (2012).